Preliminary Analysis of Nacelle for Turbofan Engine

Sharanabasappa, R. Ullas, Vivek Venkataraman Bhat and Vishwanath Koti

Abstract--- *This paper describes the study of nacelle characteristics of turbofan engine in terms of drag for various flight conditions. The nacelle cross sectional geometry was selected based on low drag aerofoil available in the literature. This aerofoil section is analyzed for various angles of attack, which are similar to engine nacelle inlet conditions. Analysis was carried out using commercial software tool called "Fluent". Appropriate boundary conditions are used along with suitable convergence criteria to get the drag characteristics. An optimum grid size and an appropriate turbulence model were selected for the analysis by varying grid size and analyzing different turbulence model. From the CFD analysis the drag and pressure recovery characteristics were derived through post processing. As an extension three dimensional sector of the Nacelle (without internal components) was meshed and analyzed for two flight conditions. From the analysis the drag characteristics of the nacelle was derived. The analyzed results show the range of flow angles for which the nacelle could operate satisfactorily.*

Keywords--- *Nacelle, CFD, Grid sensitivity, Turbulence Model, Co-efficient of lift, Co-efficient of Drag*

I. INTRODUCTION

A Nacelle is a streamline enclosure of an engine, which is attached to the aircraft wing through pylon. Nacelles are responsible for good engine performance and considerable percentage of total aircraft drag, thus fuel consumption [1]. It includes the parts commonly referred to as engine cowling, but a nacelle system encompasses other components as well including the inlet cowl, fan cowl, core cowl and nozzle as shown in Figure 1. The inlet cowl is the front lip of the engine housing, fan cowl is the leading lip for guiding mass flow to the engine. Nacelle is mainly divided into fore- body, Centre body and after body as shown in Figure 1. Fore body acts as a fan casing for the engine, centre body is where the fan casing of the engine is located. After body houses cascade thrust revere mechanism. The upper surface of the nacelle is same as the suction surface of the aerofoil where as the lower surface is having contour to match engine.

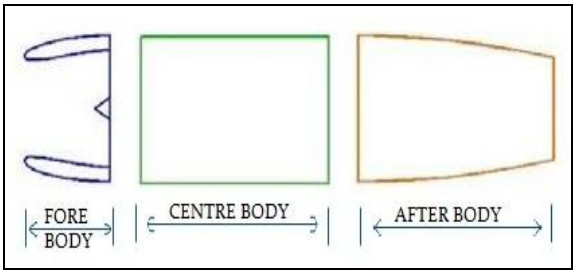

Figure 1: Different Parts of Nacelle

1.1 Nomenclature

C_D Co-efficient of drag
C_L Coefficient of lift
aoa Angle of Attack

Sharanabasappa, M.S. Ramaiah Institute of Technology, Bangalore, India. E-mail: mgsharana@gmail.com
R. Ullas, M.S. Ramaiah Institute of Technology, Bangalore, India. E-mail: ullasrudresh90@gmail.com
Vivek Venkataraman Bhat, M.S. Ramaiah Institute of Technology, Bangalore, India. E-mail: vivekvb21@gmail.com
Vishwanath Koti, Assistant Professor, Mechanical Department, M.S. Ramaiah Institute of Technology, Bangalore, India. E-mail: koti_675@rediffmail.com
PAPER ID: MEG01

P_S Local Static Pressure
P_{atm} Local Atmospheric Pressure
X Normalizing Length factor (1 Unit)
C Camber Length of an Aerofoil
X/C Normalized length of an Aerofoil
LE Leading edge of an Aerofoil
TE Tailing edge of an Aerofoil

II. 2-D ANALYSIS

2.1 Boundary Conditions

The selected aerofoil is NACA 6409. The Aerofoil was selected based on the low drag characteristics. By using this Aerofoil 2D mesh is carried out for the selected domain. The meshed domain is shown in the Figure 2. The boundary conditions are

Pressure far field: Ambient pressure, temperature and flight Mach number are specified.

Fan inlet: static pressure, temperature, density and mass flow rate are specified.

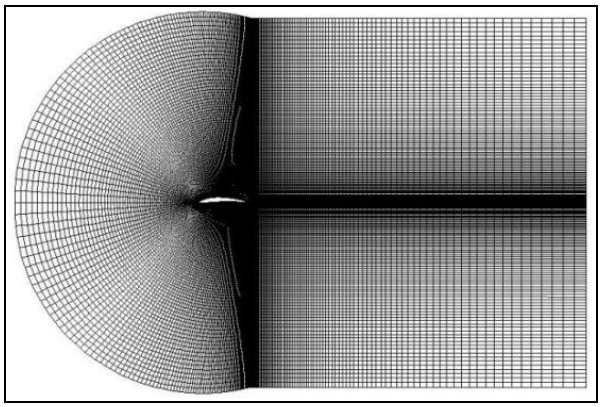

Figure 2: Meshed 2- D Domain

2.2 Selection of Grid Size

The successful flow simulation of general nacelle configuration depends on the smooth and well distributed grids in complete flow field. At the section cut of the nacelle, a C-type grid is produced using GAMBIT. The grid generated is shown in Figure 3. A grid size of 32400 elements was selected for analysis after doing grid sensitivity analysis. The C_D and C_L variation with different number of grid sizes are shown in Figures 4 and 5 respectively. It is observed from this figure that beyond 32400 elements C_D and C_L values are independent of grid size.

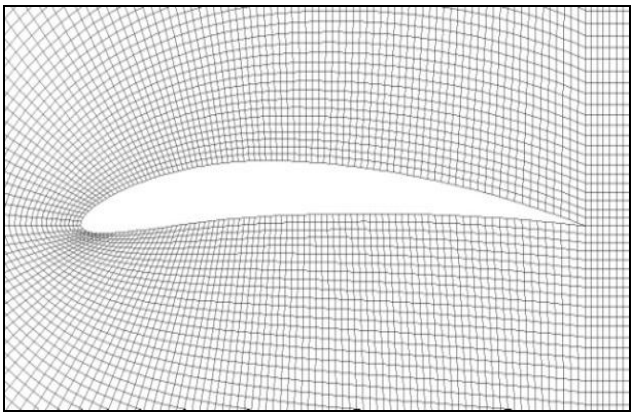

Figure 3: Grids around an Aerofoil Section(C-type)

ISBN 978-93-82338-03-1 | © 2012 Bonfring

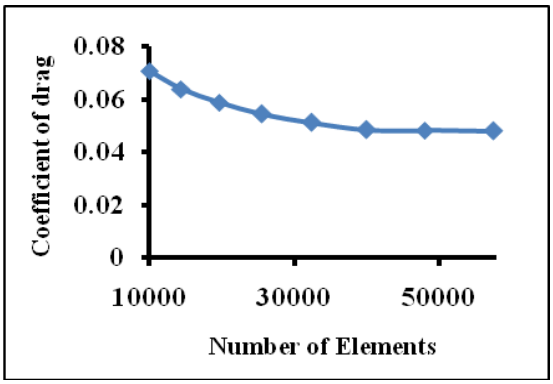

Figure 4: Convergence Criteria for Coefficient of Drag

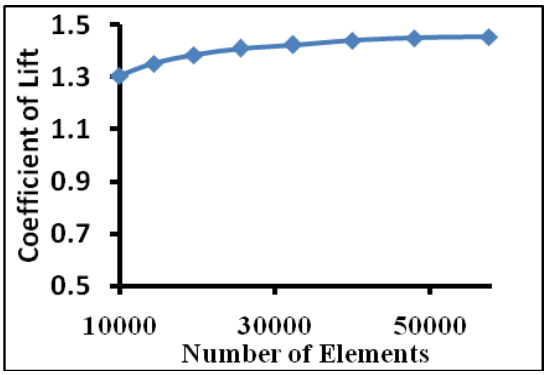

Figure 5: Convergence Criteria for Co-efficient of Lift

2.3 Selection of Turbulence Model

Turbulence is very important in the calculation of drag. Pressure and velocity will have small variations that would change to fit the turbulent flow going around any object in a flow stream. The changes have to be as accurate as possible to get the proper results.

Table 1: Different Turbulent Models

Model Number	Model Name
1	LAMINAR
2	K-EPSILON
3	SPALART-ALLAMARUS
4	REYNOLDS
5	K-OMEGA

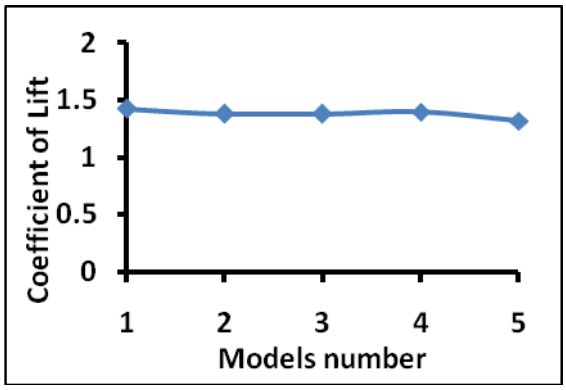

Figure 6: Co-efficient of Lift for Different Turbulence Models

ISBN 978-93-82338-03-1 | © 2012 Bonfring

Different turbulence models would give different results, and each model is suitable for different types of flow according to the conditions established. Some important turbulence models used for the present study are listed in Table1. The C_D and C_L values obtained for different turbulence models are shown in Figure-6 and Figure-7. Since the flow is turbulent the first model results are not reliable and not used. Models 2, 3 and 4 give more or less same results in C_D and C_L. Any one of these could be used for further study. However k-□ model was used. The last model namely k-omega over predicts drag. Hence this was not considered.

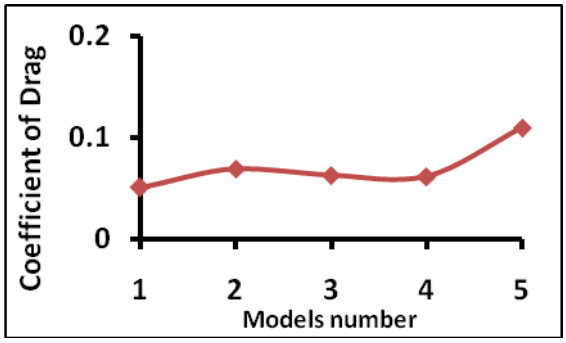

Figure 7: Co-efficient of Drag for Different Turbulence Models

2.4 2-D Results and Discussions

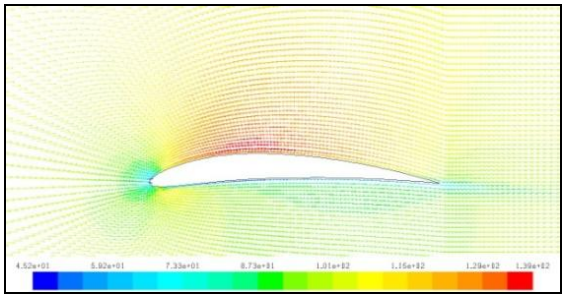

Figure 8: Velocity Contour at Sea Level for 0° Angle of Attack

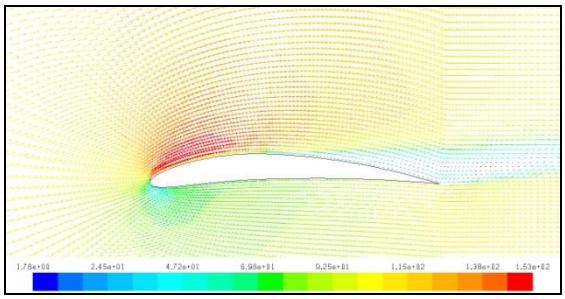

Figure 9: Velocity Contour at Sea Level for 8° Angle of Attack

The velocity contours are obtained for different angle of attack at sea level (0.3 Mach) as shown in Figures 8 and 9. The distortion is observed in the flow of the fluid over the surface of the aerofoil as the angle of attack is increased. This distortion of flow will lead to change in the flow from laminar to turbulent at location in between LE to TE. The smooth flow is observed around aerofoil at 0^0 angle of attack in Figure 8 and flow separation is observed near the trailing edge on suction side of aerofoil at 8^0Angle of Attack as shown in Figure 9. As the angle of attack increases this will lead to increase in the turbulence and hence increases the drag of system. Same analysis was carried out for cruise conditions. The pressure contours at sea level and cruise condition for 0^0angle of attack are shown in Figures 10 and 11. The minimum pressure region is shifted toward trailing edge of the aerofoil on the suction side at 0^0angle of attack for cruise condition as compared to sea level condition. This is mainly because of higher velocity the sea level.

ISBN 978-93-82338-03-1 | © 2012 Bonfring

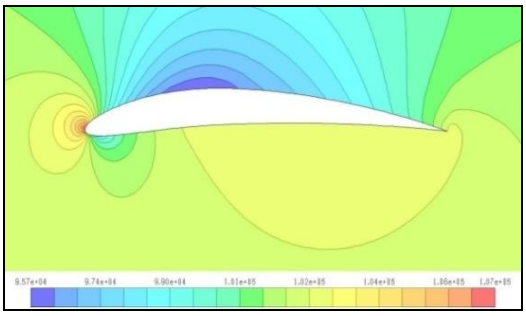

Figure 10: Pressure Contour for 0°Angle of Attack at Sea Level

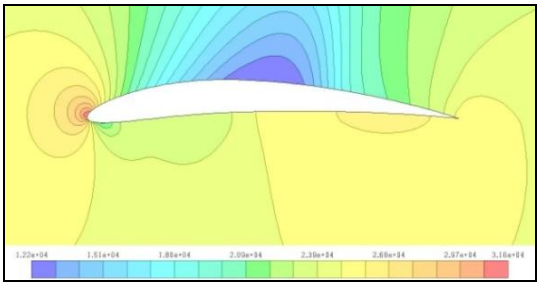

Figure 11: Pressure Contour for 0° Angle of Attack at Cruise Condition

Normalized graph for static pressure variations along chord length for both upper and lower surfaces of aerofoil at sea level (0.3 Mach) condition and cruise condition for different angle of attack are shown in Figure 12. The lower curve represents the upper surface of the airfoil. On this surface, surface static pressure is found maximum close to the leading edge then decreases suddenly to lower value and again starts rising after 2-3% of chord length and gradually increased to atmospheric level at trailing edge.

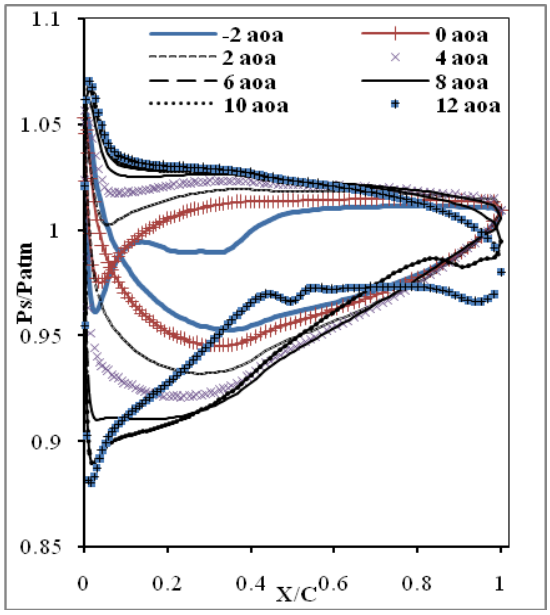

Figure 12: Ps/Patm vs. X/C for different Angle of Attack at 0.3 Mach

At cruise condition it is observed that the sudden increase in the pressure after 40% of the chord length for all angles of attack except -2^0 and 0^0 angles of attack because of the presence of shock wave. When the local Mach number becomes appreciably greater than 1, the shock wave becomes strong and the pressure distribution is radically altered as seen in Figure 13. Whereas on the pressure surface the local static pressure is found maximum at leading edge and then decreases to lower value but higher than inlet pressure and then becomes almost constant. Similar behaviour of pressure distribution on pressure side is observed for other angle of attack also. The area enclosed by the pressure curve represents the lift offered at that particular Angle of Attack. At-2^0Angle of Attack,

ISBN 978-93-82338-03-1 | © 2012 Bonfring

there is a crossing over of pressure and suction surface distribution near the leading edge indicating negative lift. This crossing point vanishes at 2^0 Angle of Attack.

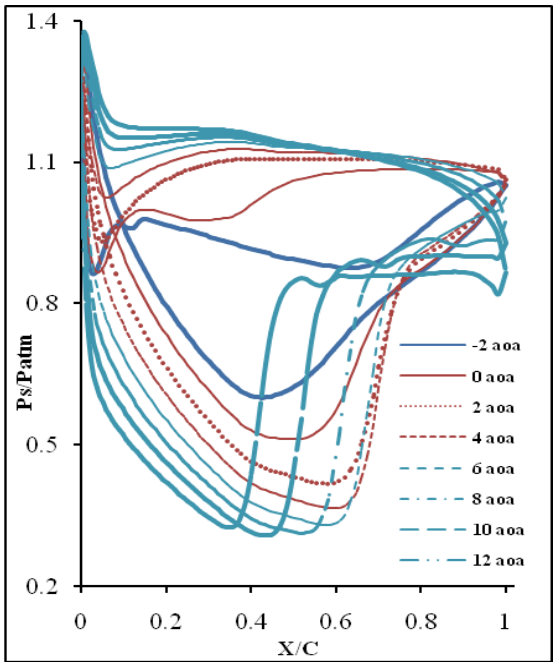

Fig 13.Ps/Patm vs. X/C for Different Angle of Attack at 0.7 Mach

The variation of Mach number over an aerofoil along chord length is shown in Figures 14 and 15 for takeoff and cruise conditions for various angles of attack respectively. The sudden decrease in Mach number is observed on the suction side of aerofoil corresponding increase in angle of attack after 2^0 due to the shock. The co-efficient of lift and drag variations with reference to various angles of attack are shown in Figures 16 and 17 respectively.

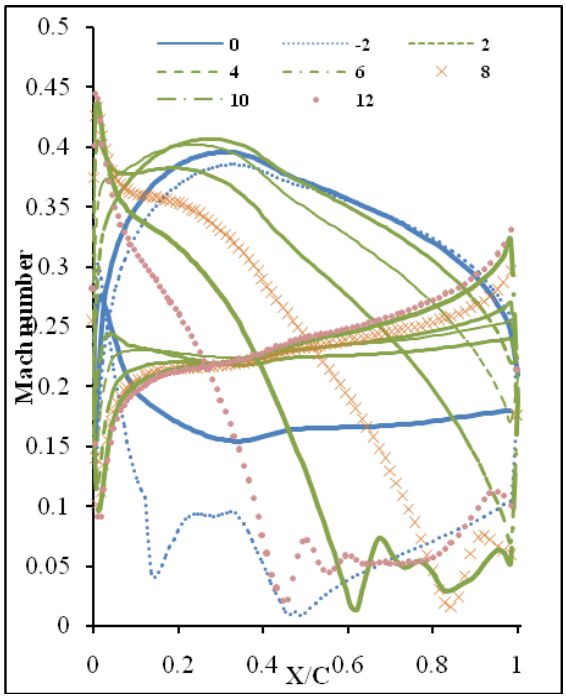

Figure14: Mach number Variation along Nacelle for Different Angle of Attack at Sea Level Condition

ISBN 978-93-82338-03-1 | © 2012 Bonfring

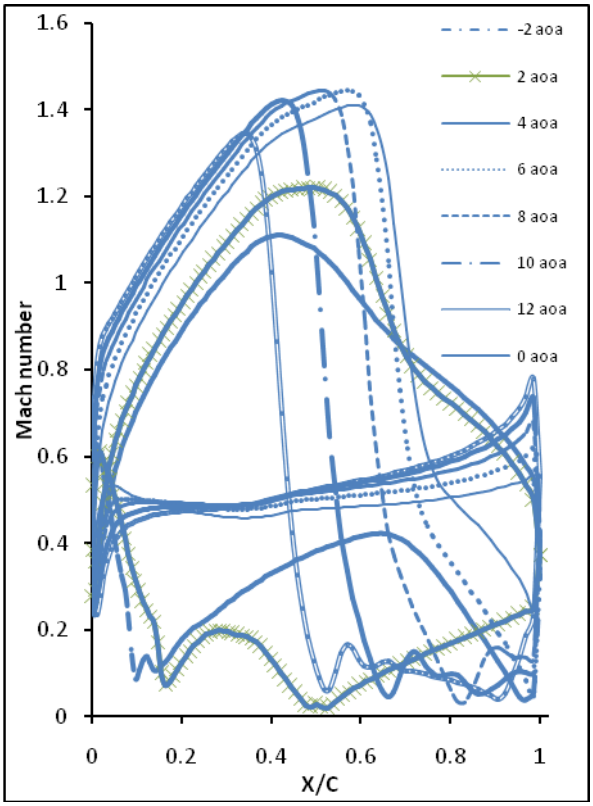

Figure 15: Mach number Variation along Nacelle for Different Angle of Attack at Cruise Condition

It is observed that the co-efficient of lift (C_L) is increased gradually corresponding increase in angle of attack up to 8^0, then the coefficient of lift decreases. At this location the co-efficient of drag (C_D) increases sharply due to flow separation. Therefore 8^0 is considered as the stalling angle for the airfoil. Increasing angle of attack beyond 8 degrees, drag increases in and the lift decreases.

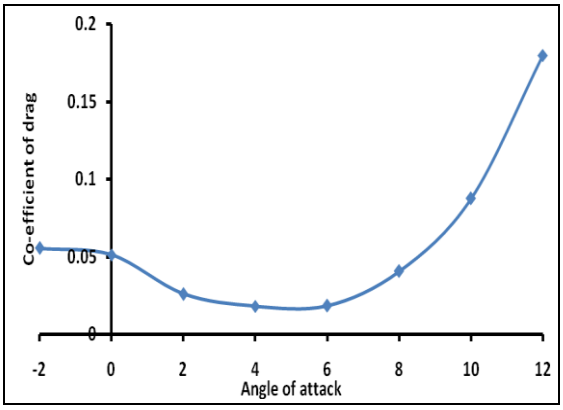

Figure 16: Coefficient of Drag Curve at 0.3 Mach

ISBN 978-93-82338-03-1 | © 2012 Bonfring

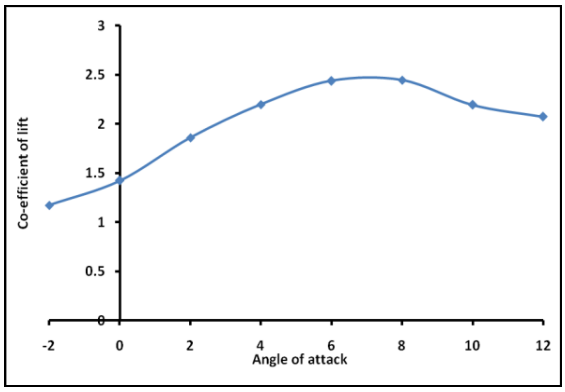

Figure 17: Coefficient of Lift Curve at 0.3 Mach

III. 3-D ANALYSIS

The geometry of the nacelle is axis-symmetric. It is possible to analyse this geometry by considering the sector of the full nacelle. Hence a 30^0 sector model was used to create the flow domain[3]. Hexahedral elements were used to generate the mesh. The finest cells were provided around to the nacelle surface and the exhaust of the nacelle and at core flow as shown in Figure 18. The static pressure variation around the cross sectional view of nacelle is shown in Figure 19.

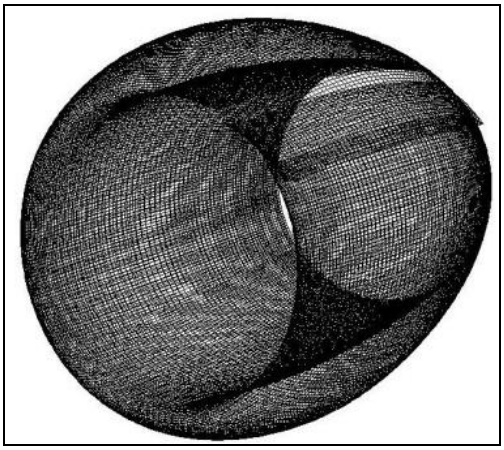

Figure 18: Enlarged View of Meshed Surface of Nacelle

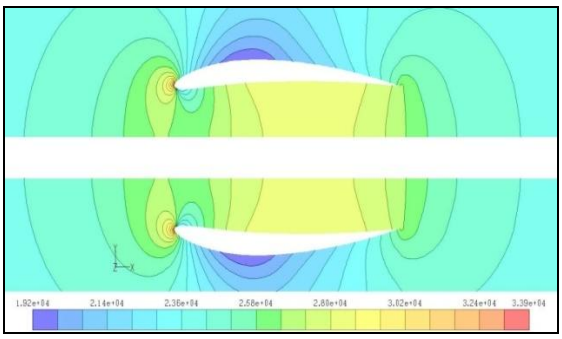

Figure 19: Pressure Contour at Cruise Condition for 0^0Angle of Attack

ISBN 978-93-82338-03-1 | © 2012 Bonfring

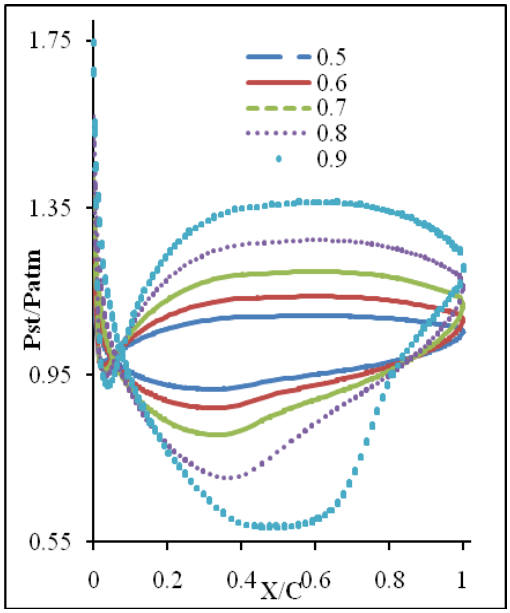

Figure 20: Pressure Variation along Nacelle for Different Mach number at Cruise Condition

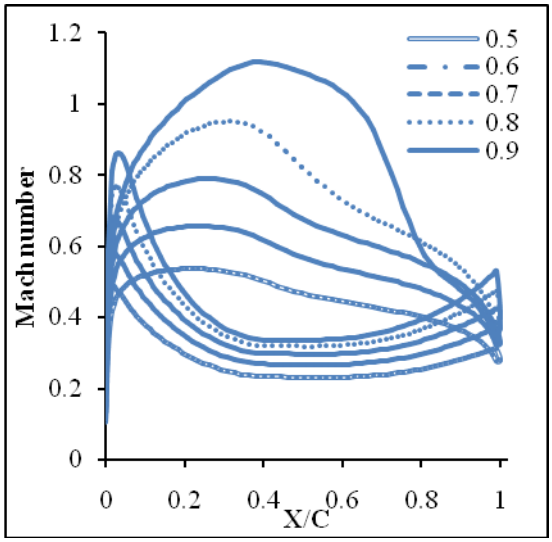

Figure 21: Mach number Variation along Nacelle for Different Mach number at Cruise Condition

3-D analysis of Nacelle was carried out at different Angle of Attack at cruise conditions (Mach number = 0.7). Converged values of Co-efficient of Drag are taken from FLUENT post-processing tools and their variations are shown in Figure 22. It is observed that as angle of attack increases from negative to higher positive values, corresponding co-efficient of drag also increases.

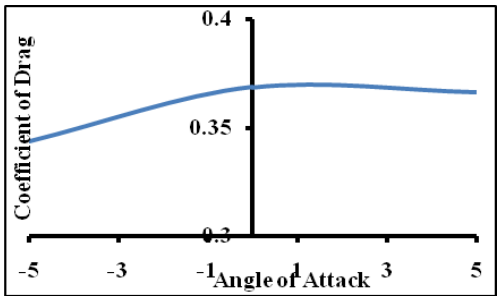

Figure 22: Co-efficient of Drag Curve for Different Angle of Attack at Cruise Condition

ISBN 978-93-82338-03-1 | © 2012 Bonfring

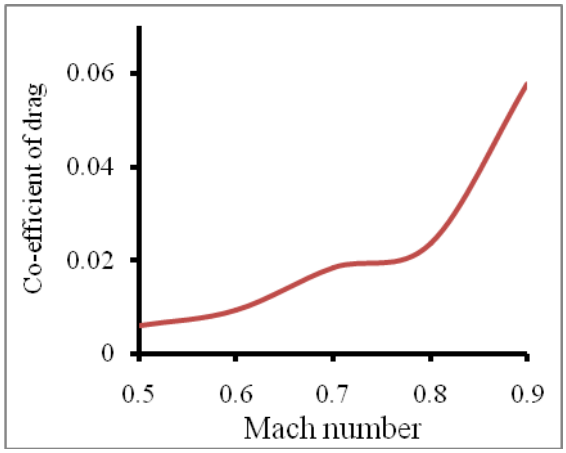

Fig 23.Co-efficient of Drag Curve for Mach number at Cruise Condition

Analysis was carried out for various cruise conditions as different Mach number in between 0.5 to 0.9. It is observed that when Mach number was increased to transonic mach, there was sharp increase in the value of coefficient of drag after 0.8 Mach number. The same result was obtained in 2-D case. It can be seen from the Fig 23, coefficient of drag is not increased much till 0.8 Mach number. But there is a sudden increase in the coefficient of drag can be observed after 0.8 Mach number.

IV. CONCLUSIONS

It was shown that 8° angle of attack is the Stall angle for the selected aerofoil NACA 6409. The pressure distributions indicate a negative lift at lower incidence. The free stream Mach number has large influence on the surface pressure distribution. The drag on the nacelle section sharply increases after stalling incidence.

ACKNOWLEDGEMENT

This content of this paper taken from the project work carried out at NCAD-NAL. The authors thank Director, NAL, Dr. S. Ramamurthy , Rajnish Kumar Singh, NCAD-NAL for the support to carry out the project.

REFERENCES

[1] Jesuino Takachi Tomita, Cleverson Bringhenti, Joao Roberto Barbosa, Antonia Batista de Jesus, "Nacelle Design for Mixed Turbofan Engines" May 2006,GT2006-91212.
[2] H.C.Chen, N.J.Yu, P.E.Rubbert, "FLOW Simulation for General Nacelle configuration using Euler Equation" 1983, AIAA-83-0539.
[3] Josue Gomez- Parada, " Parametric Analysis of the drag produced by a VHBR Engine using CFD" Oct-2009.
[4] Chen, L.T.; Yu,K.C.; Dang, " Transonic Computational Method for an Aft-Mounted Nacelle/Pylon with Power EFFECT" Journal of Aircraft 1990 0021-8669 vol27 no.10(878-885)
[5] Prat, D., Surply, T., and Gisquet, D., 1997,"Application of CFD Methods to Propulsion System Integration in the Future Supersonic Transport Aircraft", American Institute of Aeronautics and Astronautics, AIAA-97-2212
[6] Humphries, P., Gillan, M., and Raghunathan, S., 1997, "A Study of Isolated Nacelle Flows at Subsonic and Transonic Speed", American Institute of Aeronautics and Astronautics, Inc., AIAA-98-0946.
[7] Mullender, A.J. and Poll, D.I.A., 1996. "Engine Nacelle Aerodynamics". Aerospace Engineering (Warren dale, Pennsylvania), pp. 17-20.
[8] Pate, L., Lecordix, J.L. and Dessale, B., 1995. "CFD tools for designing isolated and installed nacelles", AIAA, ASME, SAE, and ASEE, Joint Propulsion Conference and Exhibit, 31st, San Diego, CA; United States; 10-12 July 1995.

ISBN 978-93-82338-03-1 | © 2012 Bonfring